Carbon 125 (2017) 93–102

Contents lists available at ScienceDirect

Carbon

journal homepage: www.elsevier.com/locate/carbon

Direct measurements of the mechanical strength of carbon nanotube - Aluminum interfaces

Chenglin Yi [a], Xiaoming Chen [a, b], Feilin Gou [a], Christopher M. Dmuchowski [a, c], Anju Sharma [d], Cheol Park [e], Changhong Ke [a, c, *]

[a] Department of Mechanical Engineering, State University of New York at Binghamton, Binghamton, NY 13902, USA
[b] Micro- and Nanotechnology Research Center, State Key Laboratory for Manufacturing Systems Engineering, Xi'an Jiaotong University, Xi'an, Shaanxi 710049, China
[c] Materials Science and Engineering Program, State University of New York at Binghamton, Binghamton, NY 13902, USA
[d] Small Scale Systems Integration and Packaging Center, State University of New York at Binghamton, Binghamton, NY 13902, USA
[e] Advanced Materials and Processing Branch, NASA Langley Research Center, Hampton, VA 23681, USA

ARTICLE INFO

Article history:
Received 18 May 2017
Received in revised form
13 July 2017
Accepted 8 September 2017
Available online 9 September 2017

Keywords:
Interfacial strength
Carbon nanotubes
Metal matrix nanocomposites
Thermal annealing
Nanomechanical testing

ABSTRACT

Interfacial load transfer plays a critical role in the bulk mechanical performance of nanofiber-reinforced metallic-matrix nanocomposites (MMNC). In this paper, we investigate the mechanical strength of interfaces in double-walled carbon nanotube (CNT)-reinforced aluminum (Al) nanocomposites by using *in situ* electron microscopy nanomechanical single-tube pull-out techniques. The nanomechanical measurements reveal the shear lag effect on the CNT-Al interface that is found to possess an average interfacial shear strength (IFSS) of about 28.7 MPa. The study also shows that thermal annealing results in substantially higher binding strength interfaces between CNTs and Al matrices. The average IFSS of CNT-Al interfaces that were thermally annealed at 400 °C is found to reach about 35.3 MPa, a 23% increase from that of the non-annealed interfaces. The maximum load bearing capacity of the annealed interfaces reaches about 304 nN, a 40.1% increase from that of the non-annealed ones (about 217 nN). The findings are useful to better understand the load transfer mechanism in CNT-reinforced MMNC and the tuning and optimization of the reinforcing performance through thermal processing.

1. Introduction

The light, strong and durable characteristics of nanofiber-reinforced metal-matrix nanocomposites (MMNC) are attractive to a number of industries such as the aerospace and automotive industries [1–3]. The nanofiber's extraordinary mechanical properties and high surface-to-volume ratio characteristics enable a substantial property enhancement of bulk metal matrix with a small amount of additive nanofibers. An adequate load transfer on the nanofiber-metal interface is essential in order to take advantage of the extraordinary mechanical properties of the reinforcing nanofibers, which is the core reinforcing mechanism in nanofiber-reinforced MMNC or nanocomposites in general [4–6]. Carbon nanotubes (CNTs) [7] are one of the most promising reinforcing fibers for disruptive MMNC technologies due to their ultra-strong, resilient and low density properties [8]. The research of CNT-reinforced MMNC first emerged in the late 1990s [9–11], and substantial advances have been achieved during the past two decades. However, the understanding of the interfacial load transfer on CNT-metal interfaces remains elusive, which has been a major scientific obstacle in the development of the CNT-reinforced MMNC technology. The underlying challenges behind the lack of such critical knowledgebase include two parts. *First*, the load transfer on CNT-metal interfaces is governed by sophisticated physical and even chemical phenomena, which possess comparable or even higher complexities compared to those involved on CNT-polymer interfaces. For examples, metal grains in direct contact with CNT lattices may yield under the shear force on the CNT-metal interface. The size/shape of metal grains and their mechanical properties are sensitive to processing conditions [12–15], which affects their contacts and interfacial interactions with CNT surfaces and thus the interfacial load transfer capacity. In addition, reaction products may form on CNT-metal interfaces at elevated processing temperatures

* Corresponding author. Department of Mechanical Engineering, State University of New York at Binghamton, Binghamton, NY 13902, USA.
E-mail address: cke@binghamton.edu (C. Ke).

http://dx.doi.org/10.1016/j.carbon.2017.09.020
0008-6223/

[16–21], and their impacts on CNT-metal bonding interactions and the interfacial load transfer remain not well-understood. The interfacial interaction is also substantially affected by the residue thermal stress on the CNT-metal interface [22–24], which is due to the fact that CNTs usually possess much lower coefficients of thermal expansion (CTEs) than metal materials. Dislocation plays an important role in metal strengthening, which are substantially affected by the residue thermal stress as well as the Orowan looping effect due to the small size of CNTs [25]. *Second,* it is technically challenging to directly and quantitatively characterize the interfacial load transfer on CNT-metal interfaces at an *individual* tube level. Direct quantitative measurements of the interfacial strength of individual nanotubes with metal matrices are essential for a complete understanding of the interfacial stress transfer and their reinforcing mechanisms. However, a vast majority of the reported studies on CNT-reinforced MMNC in the literature were carried out at a macroscopic level, which can at most be used to evaluate interfacial strength properties indirectly and qualitatively [21,23,26–29]. Reports on direct, quantitative, and microscopic measurements of the interfaces formed by individual nanotubes with metal matrices remain scarce [16,30]. This is ascribed to the challenges in the nanomechanical characterization that requires precise nano positioning and manipulation with adequate spatial resolutions, applying and sensing loads with adequate force resolutions, and real-time observation of the mechanical response of nanostructures that typically demands *in situ* electron microscopy techniques [31,32]. The preference of using small diameter nanotubes (e.g., single or double-walled nanotubes) for MMNC applications tends to add an additional degree of challenges in the nanomechanical measurement of tube-metal interfaces in MMNC. This is because in nanotube-reinforced MMNC, only the outermost shell of a tube makes contacts with metal matrices and contributes to effective load transfer, and thus the property enhancement of the matrix.

In this work, we investigate the mechanical strength of interfaces in CNT-reinforced aluminum (Al) nanocomposites by using *in-situ* electron microscopy nanomechanical single-tube pull-out techniques. Aluminum is chosen as the model matrix material for this study due to its widespread usage in the aerospace and automotive industries. By pulling out individual double-walled CNTs of 3.1 nm in median diameter with different embedded lengths, the measurements reveal, *for the first time*, the shear lag effect on the CNT-Al interface and demonstrate that the effective interfacial load transfer occurs only within a certain embedded length. The nanomechanical study further reveals quantitatively that thermal post-processing leads to a substantial increase of the interfacial strength in CNT-Al nanocomposites, which is in part ascribed to a more intimate contact between CNT surfaces and Al grains that is caused by the residue thermal stress. The findings are useful to better understand the load transfer mechanism in CNT-reinforced MMNC and provide new insights into the reinforcing performance optimization through facile thermal treatments. The experimental methodologies established in this work can be readily extended to study the interfacial load transfer in other MMNCs that are composed of CNTs or other one-dimensional (1D) reinforcing fibers (e.g., boron nitride nanotubes) with a wide selection of metal matrices and their alloys.

2. Results and discussion

2.1. In situ electron microscopy nanomechanical single-tube pull-out measurements

Fig. 1(a) illustrates the employed *in situ* electron microscopy single-tube pull-out technique. In this testing scheme, the tested CNT-metal interface is formed inside a sandwiched metal/CNT/metal thin-film nanocomposite. A pre-calibrated atomic force microscopy (AFM) cantilever acts as a force sensor, and is mounted vertically to the stage of a 3D piezo nanomanipulator. The tip of the AFM probe is controlled to first grip the free-end of an identified protruding CNT cantilever with the aid of electron beam induced deposition (EBID) of Pt. Then, an incrementally increasing tensile force is applied to the tube through displacing the AFM cantilever until the nanotube is fully pulled out from the composite. The nanomechanical measurement is performed *in situ* inside a high resolution scanning electron microscope (HRSEM). The high resolution electron beam is used to control and monitor the whole manipulation process and the mechanical response of the tested tube during the pull-out process. This nanomechanical single-tube pull-out scheme is envisioned to be capable of testing tube-metal interfaces for a broad selection of metal materials and for tubes/fibers with a broad range of diameters (e.g., from a few to hundreds of nm). A similar version of this technique, in which metal matrices are replaced by polymer matrices, was demonstrated in the recent studies of the load transfer in nanotube-reinforced polymer nanocomposites [31,33,34].

Fig. 1(b) illustrates the main processes of manufacturing CNT-Al sandwiched thin nanocomposites with the engineered CNT-Al interfaces for the single-tube pull-out test as illustrated in Fig. 1(a). In brief, a thin layer of Al is first deposited on a clean silicon substrate (b-1), followed by the deposition of a well-dispersed CNT solution (b-2). Subsequently, a second Al layer is deposited on top to form an Al/CNT/Al thin-film nanocomposite (b-3). An optional step here is to have the thin-film nanocomposite thermally annealed in air at up to 400 °C. The thin-film nanocomposite is then fractured through cutting the substrate using a diamond cutter, and some of the embedded tubes are partially exposed as free-standing cantilevered structures (b-4). The advantage of this sample preparation approach is that a whole tube (including both the embedded and the protruding segments) stays in one horizontal plane, and is able to maintain its straightness if its length is controlled to be relatively short. It is noted that Al is an active material and reacts spontaneously with the contact of air and/or water. It is anticipated that a thin oxide layer is formed on the top surface of the first deposited Al film. Because the Al deposition is performed in an ultra-high vacuum environment. The oxide layer is not expected to appear in the contact between CNTs and the 2nd deposited Al film, which is considered as a contact between pure Al grains and CNTs. As displayed in the cross-section drawing in Fig. 1(b-4), the contact region between the CNT and the Al_2O_3 layer is expected to be much smaller than its contact with the surrounding Al grains. Therefore, the impact of the existence of the oxide layer on the overall load transfer on the CNT-Al interface is expected to be limited.

Fig. 2(a) shows an AFM image of a freshly deposited Al film of 100 nm in thickness on a silicon substrate by using electron beam evaporation deposition methods (see Materials and methods section for details). Fig. 2(b) shows an AFM image of a 100-nm-thick Al film that was thermally annealed at 400 °C for 2 h. The grain size of the annealed film is noticeably larger than that of the non-annealed one. For the grains shown in the two AFM images, the average grain size of the annealed film is estimated to be 32% larger than that of the non-annealed film. The X-ray photoelectron spectroscopy (XPS) characterization of the Al films, which is displayed in Fig. 2(c), shows that a thin-layer oxide of about 2 nm in thickness was formed on freshly deposited Al films, while a thicker oxide layer of about 7 nm was formed for thermally annealed Al films. XPS was employed to monitor changes in the surface aluminum oxide thickness between freshly deposited Al films with the ones thermally annealed at 400 °C for 2 h. The Al(2p) spectra shown in Fig. 2(c) clearly show an increase in the intensity of the oxide

component at high binding energy and a corresponding decrease in the metal component of the thermally annealed sample. Oxide film thickness was estimated from the XPS data by assuming a uniform smooth film on the substrate, which was confirmed independently with spectroscopic ellipsometry measurements. A native oxide of about 2.0 nm is estimated on the freshly deposited Al films, while the aluminum oxide thickness increased to about 7.0 nm on the 400 °C annealed film. Double-walled CNTs (DWCNTs) with a polydispersed diameter are employed in this study. Prior AFM studies reveal that a majority of the tubes (>90%) possess an outer diameter within 2–4.2 nm with a median diameter of 3.1 nm [33]. The nanotube length is a key parameter in the sample preparation and was controlled through adjusting the ultrasonication time during the dispersion process. AFM studies, which are represented by the insert image shown in Fig. 2(a), reveal that tubes of less than 2 μm in length are capable of maintaining reasonable straightness when deposited on the Al film by spin-coating. Fig. 2(d) shows one of the manufactured Al/CNT/Al sandwiched thin-film nanocomposites with several protruding nanostructures. High resolution transmission electron microscopy (HRTEM) inspection confirms that those protruded structures are indeed carbon nanotubes with clean surfaces that are free of any attached Al grains residues. Fig. 2(e) shows an HRTEM image of one representative protruding tube of 3.2 nm in outer diameter from a CNT-Al nanocomposite film. The materials surrounding the embedded tube segments were confirmed to be aluminum based on the energy-dispersive X-ray (EDX) spectroscopy characterization as exemplified by Fig. 2(f).

Fig. 3(a)–3(c) show three selected SEM snapshots of one representative single-tube pull-out measurement by using the manufactured sandwiched CNT-Al nanocomposite samples. To ensure that a tube was loaded and pulled out by a tensile force, only those tubes that were oriented perpendicular to the AFM cantilever back surface were selected for pull-out measurements. The EBID of platinum (Pt) [35] was employed to ensure a firm attachment between the free end of the nanotube and the AFM tip. The pull-out of the nanotube was observed to occur as a catastrophic failure of the CNT-metal interface when the stretching force reached a certain value (i.e., pull-out force). For this measurement, the pull-out force and the embedded tube length are measured to be about 219 nN and 1.05 μm, respectively. It can be clearly seen that the EBID-deposited Pt also covered the protruding portion of the tube through diffusion and resulted in a noticeable lateral size increase. However, it is expected to have no influence on the tube-metal interface and thus the interfacial strength measurement. The presence of the Pt layer on the protruding portion of the tube acts favorably as an aid for the determination and measurement of the embedded tube length.

Interface failure scenarios other than the successful single-tube pull-out like the one shown in Fig. 3 were also observed and were categorized as tube fracture and telescopic pull-out, which are exemplified by the selected SEM snapshots shown in Fig. 4(a) and (b), respectively. It is noted that the observed fracture of the tube occurred in the protruding tube segment, while the telescopic pull-out occurred as a result of the breaking of the outermost tube shell that was in direct contact with the metal matrices at the interface by the stretching force and subsequently pull-out of the inner tube shells. It is noted that fracturing of the outermost tube shell is a clear sign of effective load transfer in nanofiber reinforced nanocomposites [36]. The observed telescopic pull-out phenomenon provides direct and convincing evidence for the reinforcing mechanism of CNTs in MMNC through effective interfacial load transfer [37]. In both scenarios, the tested tube-metal interfaces remained intact. It is noted that the protruding nanotube was exposed to the electron beam throughout the entire experimental session. Therefore, the electron beam irradiation might have a material effect on the strength of protruding nanotubes, and is a plausible factor that accounts for the observed tube fracture and telescopic pull-out scenarios. However, because the tested nanotube-metal interface was buried under a metal film of about 100 nm in thickness and not exposed directly to the electron beam, the electron beam irradiation was expected to have little or no effects on the nanotube-metal interfacial strength. The occurrences of these scenarios were clearly visualized from the recorded HRSEM images, and thus they are excluded from the mechanical strength analysis of the CNT-metal interface.

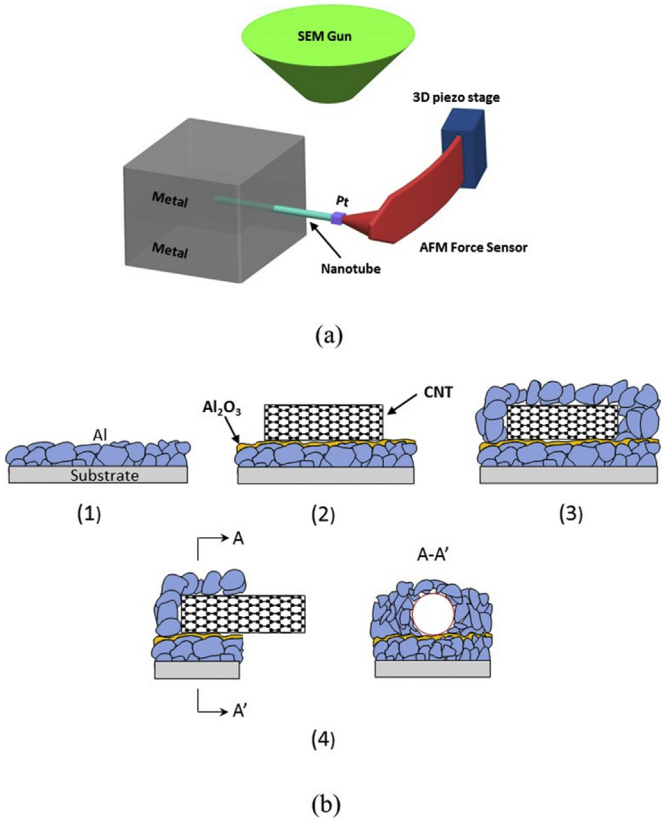

Fig. 1. **(a)** Schematic of the *in situ* nanomechanical single-tube pull-out testing technique inside a high resolution scanning electron microscope. The tested nanotube-Al interface is inside an Al/nanotubes/Al sandwiched thin-film nanocomposite. **(b)** Schematics of the manufacturing processes of Al/nanotubes/Al sandwiched thin-film nanocomposites and protruding nanotube samples. The drawings are not to scale. (A colour version of this figure can be viewed online.)

Fig. 5 shows the pull-out forces measured in 36 different single-tube pull-out tests with the embedded tube length ranging from about 73 to 1608 nm. Among them, 18 measurements were performed on CNT-Al samples without any post thermal treatments, while the other 18 were on thermally annealed CNT-Al samples. Both sets of data display a similar trend in the dependence of the pull-out load on the embedded tube length: the pull-out force first increases, in a nearly linear relationship with the embedded length, and then forms a plateau where the force falls into a fairly narrow range even as the embedded length further increases substantially. The measured data sets are first fitted using bilinear curves, which are also displayed in Fig. 5. The force plateau of the thermally annealed CNT-Al interface is calculated to be 304 ± 10 nN and is about 40.1% higher than that of the interfaces without thermal treatments (217 ± 8 nN). The results clearly show that the process of thermal annealing at 400 °C did not result in any material degradation of the structural and mechanical properties of the tested

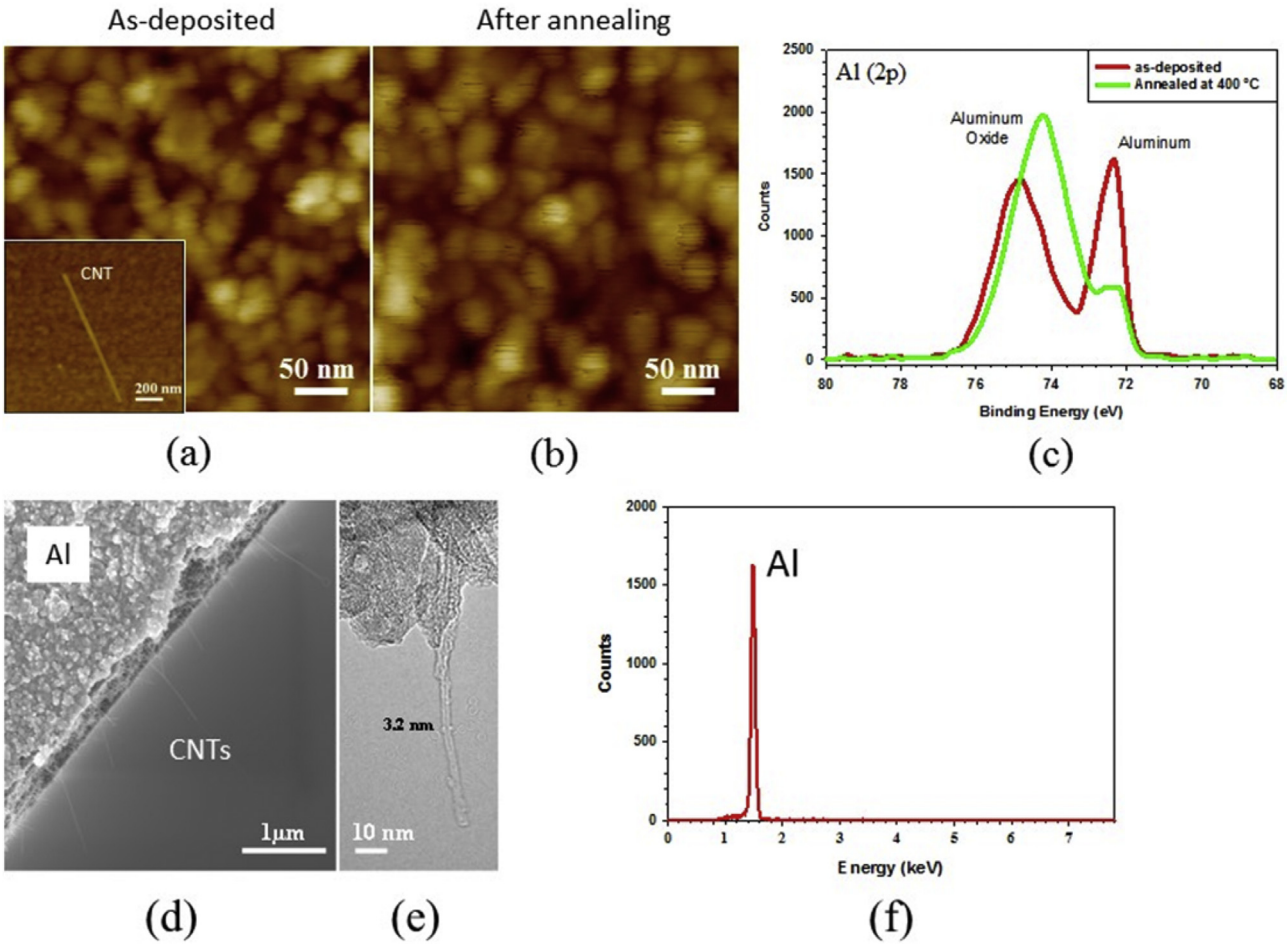

Fig. 2. Characterization of Al thin films that were deposited by using electron beam evaporation methods and the manufactured Al-CNT nanocomposites. AFM images of **(a)** as-deposited and **(b)** thermally annealed Al thin films. The insert image in (a) shows one CNT of about 3 nm in diameter and about 1.1 μm in length that was deposited on an Al surface by using spin coating. (**c**) Representative XPS spectra of as-deposited and thermally annealed Al films. (**d**) A fractured CNT-Al thin-film nanocomposite showing several protruding CNTs. (**e**) High resolution TEM image of one protruding CNT of 3.2 nm in outer diameter from a CNT-Al composite. (**f**) Representative EDX spectrum of the matrix materials (Al) in the regions surrounding the embedded tube segments. (A colour version of this figure can be viewed online.)

CNTs, which otherwise would not be able to hold the higher stretching force applied to the annealed samples. The dependence of the measured pull-out force on the embedded tube length as displayed in Fig. 5 is a clear sign of the shear lag effect, which describes the shear load transfer behavior on the tube-metal interface and is one of the major energy dissipation mechanisms in nanofiber reinforced nanocomposites. When a partially embedded tube is gradually stretched at its free end, the shear stress starts to build up on the tube-matrix interface. The resulting shear stress on the tube-matrix interface has a non-uniform distribution, and possesses its maximum value at the tube entry position and then decays rapidly toward the embedded tube end. When the maximum shear stress exceeds a critical limit, a crack initiates and then propagates through the entire tube-matrix interface, leading to a catastrophic pull-out event as observed in our nanomechanical measurements. It is noted that the required pull-out load for the crack-initiated interfacial debonding remains unchanged if the embedded tube length exceeds a threshold value that is named as “critical embedded length”. Here, this critical embedded length is estimated as the length corresponding to the intersection point of the bilinear fitting curve and is calculated to be about 780 nm for non-treated Al-CNT interfaces and about 950 nm for thermally annealed interfaces, respectively. To the best of our knowledge, our nanomechanical measurements capture, *for the first time*, the shear lag effect on the CNT-metal interfaces in experiments. The shear lag effect is of importance to a complete understanding of the interfacial load transfer on tube-metal interfaces. The shear lag effect indicates that an effective interfacial shear load transfer between a nanotube and a metal interface occurs only within the critical embedded length range and any further increase of the embedded length does not contribute to the shear load bearing capacity of the tube-metal interface. It is worth mentioning here that the contacts between the CNT surface and the surrounding Al grains as illustrated in the drawing in Fig. 1(b) are likely spotty. The actual contact areas between the CNT surface and Al grains that effectively contribute to the interfacial load transfer might be smaller than the values based on the measured embedded length.

2.2. Quantification of the interfacial shear stresses on CNT-Al interfaces

In this section, two types of interfacial shear stress (IFSS) are quantified based on the single-tube pull-out measurements: (a) the average IFSS that is defined based on an assumed uniform shear stress distribution along the whole embedded tube length; (b) the maximum IFSS that occurs at the tube entry position. It is noted that actual distribution of the shear stress along the tube-metal interface is non-uniform in nature and the maximum shear stress

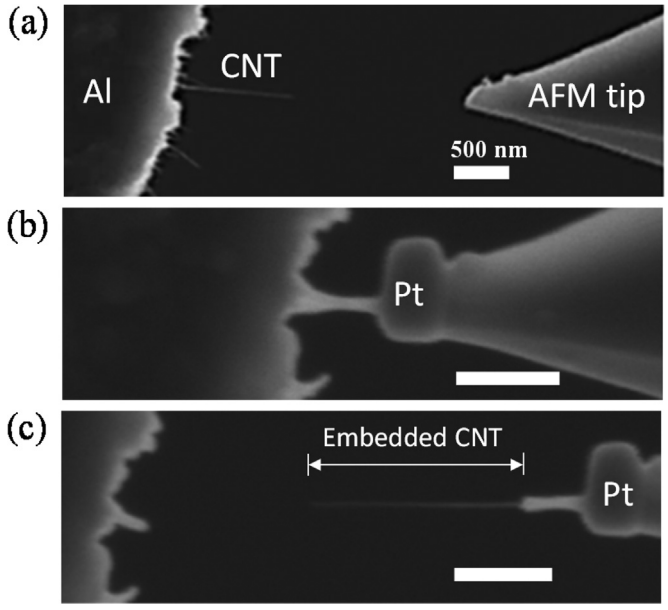

Fig. 3. Selected high resolution SEM snapshots showing the key processes in one representative single-tube pull-out measurement. **(a)** The AFM tip was controlled to approach and then touch the free end of one selected protruding CNT that was oriented perpendicular to the AFM cantilever back surface. **(b)** The free-end of the protruding tip was welded to the AFM tip by means of electron beam induced deposition of Pt. **(c)** The embedded segment of the CNT was completely pulled-out of the metal matrix by applying a tensile force. All scale bars represent 500 nm.

always occurs at the tube entry position. The average IFSS is only meaningful for shorter embedded tube lengths that are below the value of the critical embedded length.

2.2.1. The average interfacial shear stress

The average IFSS, τ_{ave}, is calculated as the slope of the initial linearly increasing fitting curve and is given as $\tau_{ave} = \frac{P}{\pi \times D \times l}$, in which P is the pull-out force, D is the diameter of the tube, and l is the embedded tube length. In our experiments, the diameters of the tested tubes could not be measured precisely as they approach the resolution limit of the electron beam. Here we evaluate the IFSS based on the measured median tube diameter (i.e., $D = 3.1$ nm) and the data, which are listed in Table 1, are deemed as the most representative values of the CNT-Al interfacial strength. Table 1 also includes the IFSS data that are calculated based on the upper and lower diameter limits of the employed tubes that were obtained from AFM studies. The average IFSS of the thermally annealed interfaces is calculated to be 35.3 ± 6.2 MPa based on the median tube diameter, about 23% higher than that of the interfaces without thermal treatments (28.7 ± 3.4 MPa). The data for the non-treated interface are generally consistent with the values 24.8 ± 3.2 (MPa) recently reported by Kawasaki and co-workers [30] that were based on measurements of CNT-Al interfaces formed using multi-walled CNTs of 20–110 nm in diameter. The slightly higher median value of our work as compared with the value reported by Kawasaki et al. is likely a sign that CNTs of small diameters and fewer numbers of walls may be capable of forming more intimate contacts with the surrounding aluminum grains because of their lower bending and transverse rigidities that enable them deform more readily under the CNT-Al interfacial binding interaction. The combination of the larger surface-to-volume ratio and higher interfacial load transfer capacity suggests that thin CNTs, such as the DWCNTs employed in this study, are of substantial technological advantages for MMNC technologies.

2.2.2. The maximum interfacial shear stress

In this section, we present a continuum mechanics model to analyze the interfacial load transfer on the tube-metal interface and to quantify the maximum IFSS that occurs at the tube-entry positon. It is noted that pure aluminum reportedly possesses a yield stress (in tension) of only about 39 MPa [38] and a corresponding yield shear stress of only about 22.5 MPa. Therefore, the aluminum grains, in particular, those in the direct contact with nanotube surfaces or in the vicinity of the contact region may yield under the interfacial shear stress during the pull-out process. Here, we present a simplified shear-lag model that takes into account the yielding of the metal films, which is illustrated by the drawings shown in Fig. 6.

A uniform interface is assumed to be formed by CNT surfaces with pure aluminum grains along the entire embedded tube length, while their contact with the Al_2O_3 layer on the top of the bottom Al layer is neglected here. This simplification is justified because of the small contact region between CNT surfaces and the Al_2O_3 layer as compared with their contact with the surrounding pure aluminum

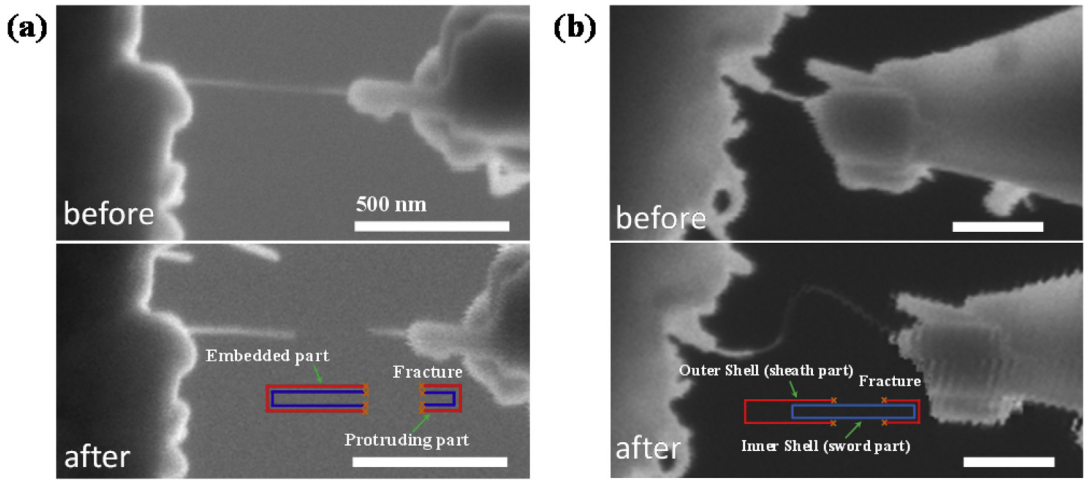

Fig. 4. Selected SEM snapshots demonstrating the two types of observed failure modes during the single-tube pull-out measurements: (**a**) fracture of a nanotube; (**b**) telescopic pull-out of a nanotube. The insert schematics illustrated the respective tube failure mechanisms. All scale bars represent 500 nm. (A colour version of this figure can be viewed online.)

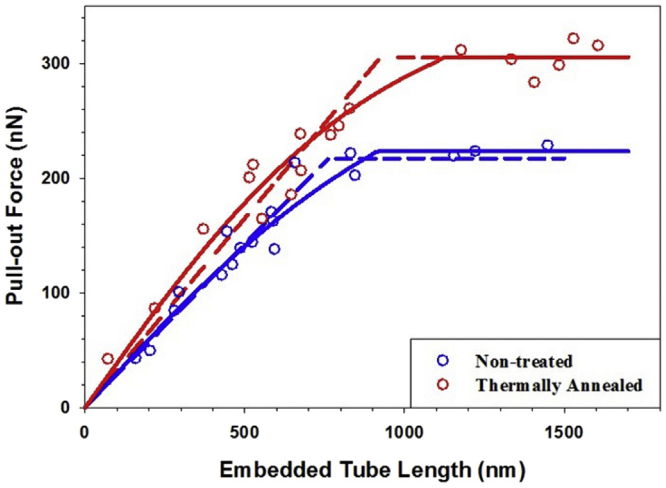

Fig. 5. The measured dependences of the pull-out force on the embedded tube length for both as-prepared/non-treated (blue dots) and thermally annealed (red dots) CNT-Al interfaces. The dashed lines are the bilinear fitting curves to the respective data sets. The solids lines are the respective fitting curves predicted by using the shear-lag model. (A colour version of this figure can be viewed online.)

grains. In addition, the deformation in the aluminum matrix caused by the interfacial shear stress is assumed to be pure shear and to occur only within a thin aluminum layer that is in direct binding contact with the CNT surface [39], which is marked as the shaded area in the illustration drawing in Fig. 6(b). When an incrementally increasing stretching force is exerted on the protruding CNT, the interfacial metal layer first experiences pure elastic shear deformations if the interfacial shear stress is below its yield shear stress. The plastic shear deformation is expected to initiate from the tube entry position when the interfacial shear stress reaches and exceeds its yield shear stress. Both the increase of the maximum shear stress at the tube-metal interface and the propagation of the plastic deformation zone are driven by a further increase of the external stretching force. Cracks initiate at the tube entry position and then propagate through the whole embedded length, resulting in a catastrophic failure of the tube-metal interface in the form of tube pull-out, when the maximum shear stress exceeds the critical limit. The equilibrium equation for the embedded tube segment is given as

$$\sigma_z \cdot \pi D^2 + 4 \int_{z_0}^{z} \tau_i \pi \cdot D dz = 0. \tag{1}$$

where z is the coordinate axis along the tube length with z_0 as the position of the tube end. σ_z is the normal stress in the tube and is given as $\sigma_z = E_f \frac{du(z)}{dz}$, in which E_f is the Young's modulus of the nanotube and $u(z)$ is the displacement of the tube; τ_i is the interfacial shear stress. A bi-linear stress-strain relationship is assumed for aluminum. The interfacial shear stress in the elastic deformation region $(z_0 \le z \le z_P)$ and the plastic deformation region $(z_P < z \le l)$ of the interfacial metal layer is given as [39]

$$\tau_i = \begin{cases} K_1 \cdot u(z), & z_0 \le z \le z_P \\ K_2 \cdot [u(z) - u(z_P)] + \tau_Y, & z_P < z \le l \end{cases} \tag{2}$$

where τ_Y is the yield shear stress of aluminum; K_1 is a coefficient related to the material properties of aluminum and the thickness of the interfacial metal layer (denoted as t) in the elastic deformation region and is given as $K_1 = \frac{E_{Al}}{2(1+\nu_{Al}) \cdot t}$, in which ν_{Al} is the Poisson's ratio of aluminum; K_2 is a coefficient related to the shear deformation of the interfacial metal layer after yielding and is given as $K_2 = \frac{G^p_{Al}}{t}$, in which G^p_{Al} is the plastic shear modulus of aluminum. By inserting the relationships in Equation (2) into Equation (1), the governing equations in both the elastic and plastic regions of the interface metal layer are given as

$$\pi D^2 \cdot E_f \frac{d^2 u(z)}{dz^2} + 4\pi D K_1 u(z) = 0, \quad z_0 \le z \le z_P \tag{3a}$$

$$\pi D^2 \cdot E_f \frac{d^2 u(z)}{dz^2} + 4\pi D \{K_2 [u(z) - u(z_P)] + \tau_Y\} = 0, \quad z_P < z \le l \tag{3b}$$

The boundary conditions used in the model include: $\sigma_z = 0$ at $z = 0$ and $\tau_i = \tau_Y$ at $z = z_P$. It is noted that the thickness of the interfacial metal layer (t) and the coefficient K_2 are obtained through fitting the experimentally measured values of the pull-out force and the tube embedded length as presented in Fig. 5. Equations (3a) and (3b) are solved numerically with the following parameters: $E_{Al} = 69$ GPa, $\tau_Y = 22.5$ GPa, and $\nu_{Al} = 0.3$ for aluminum; $E_f = 1$ TPa and $D = 3.1$ nm for CNTs.

The theoretically predicted pull-out force vs the embedded tube length relationships are plotted as solid lines in Fig. 5 and are in good agreement with the experimental measurements for both thermally treated and non-treated samples. The calculation of the two theoretical curves are based on the following values of the two fitting parameters: $t = 2.5$ nm and $K_2 = 8.9 \times 10^{14}$ N/m^3 for thermally treated interfaces or 6.9×10^{14} N/m^3 for non-treated interfaces. Three distinct relationships are displayed in the theoretically predicted curves. The linear relationship of the pull-out force vs embedded tube length occurs only at relatively shorter embedded lengths (i.e., up to about 400 nm) for both types of samples. The increase of the tube embedded length results in a nonlinear relationship with a gradually decreasing slope, until the pull-out force approaches a constant value forming a flat plateau in the curve. Here, the critical embedded length is quantified from the theoretical curve as the length value that corresponds to a pull-out load that is 1% below the plateau value and is found to be about 1100 nm for thermally treated CNT-Al interfaces, and about 900 nm for non-treated interfaces. Both values are about 15% higher than the respective values estimated from the bi-linear fitting curves.

The distribution of the shear stress on the CNT-Al interfaces is also obtained and displayed in Fig. 7 for two representative embedded lengths that are chosen to be 200 nm longer than the respective critical embedded lengths. The plots show that substantial yield deformation occurs in the interfacial metal layer when the pull-out events occur, while the elastic deformation region is relatively short (about 200 nm for both cases). The maximum shear stress is calculated to be about 40.1 MPa for thermally treated CNT-Al interfaces, and about 31.0 MPa for non-treated CNT-Al interfaces, both of which are based on the median tube diameter. It is noted that the calculated maximum shear stress is about 13.6% higher than the calculated average shear stress for thermally treated samples, while about 8% higher for non-treated samples. The predicted values of the maximum shear stress and the estimated critical embedded length by using the shear-lag model are presented in Table 1.

2.3. Analysis of the effects of thermal annealing on the interfacial load transfer

The nanomechanical measurements and the calculated IFSS values clearly reveal that the thermal processing has a substantial impact on the load transfer and load bearing capacity of the CNT-Al interface. It has been widely known that the mechanical properties

Table 1
The summary of the measured pull-out force, the estimated critical embedded length, and the calculated interfacial shear strengths (IFSS) of the CNT-Al interface based on the *in-situ* single-tube measurements. The average and maximum IFSS values are calculated based on the lower limit (2.0 nm), the median (3.1 nm) and the upper limit (4.2 nm) of the nanotube diameter range measured by AFM, respectively.

CNT-Al interfaces	Bi-linear fitting					Shear-lag model				
	Maximum pull-out force (nN)	Estimated Critical tube embedded length (nm)	*Average* interfacial shear strength (MPa)			Maximum pull-out force (nN)	Estimated Critical tube embedded length (nm)	*Maximum* interfacial shear strength (MPa)		
			2.0 nm	3.1 nm	4.2 nm			2.0 nm	3.1 nm	4.2 nm
Non-treated	217 ± 8	780	42.5 ± 5.6	28.7 ± 3.4	21.2 ± 2.4	223 ± 5	900	79.3 ± 3.3	31.0 ± 1.8	24.1 ± 1.6
Thermally Annealed	304 ± 10	950	53.8 ± 10.5	35.3 ± 6.2	25.1 ± 4.6	304 ± 10	1100	95.1 ± 5.5	40.1 ± 3.1	26.3 ± 2.4

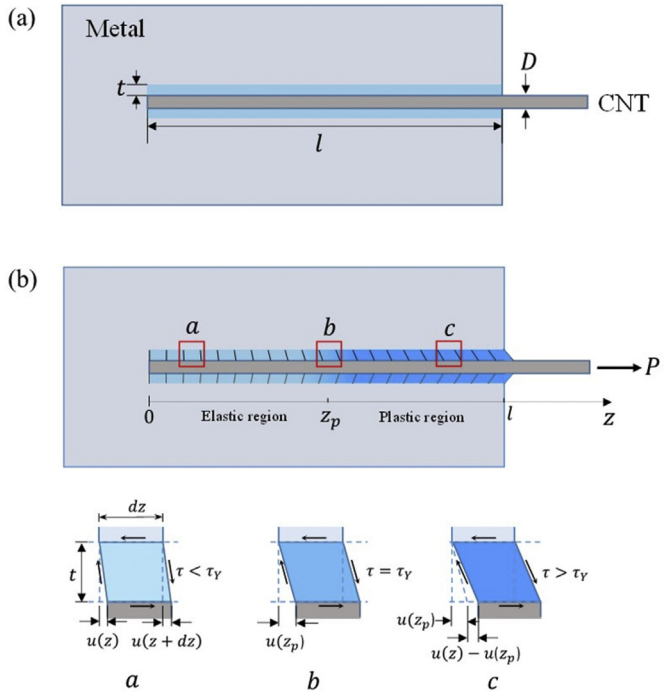

Fig. 6. Schematic illustration of the shear lag model and interfacial shear stress on the CNT-metal interface. The shaded region (in blue) represents an interfacial metal layer. (**a**) The undeformed CNT-Al interface configuration; (**b**) The deformed CNT-Al interface configuration with the interfacial metal layer under pure shear deformations, which are visualized with the aid of the added short mesh lines and three representative free-body diagrams for elements in the elastic, onset of yielding, plastic regions, respectively. (A colour version of this figure can be viewed online.)

of Al matrices and CNT-Al nanocomposites can be readily altered by thermal annealing. However, the exact effect of the thermal processing on the interfacial strength in CNT-Al nanocomposites is hard to elucidate based on the bulk measurements. This is because the bulk mechanical properties of CNT-Al nanocomposites are influenced by several factors other than interfacial load transfer, such as CNT dispersion and alignment, which are hard to control and quantify. The *in situ* nanomechanical single-tube pull-out measurements as presented in this work provide a convincing venue for quantifying the effect of the thermal processing on the load bearing capacity of the CNT-metal interface. Here we discuss the possible mechanism that accounts for the observed increase of the IFSS for thermally annealed CNT-Al interfaces. The first and most likely source of the mechanism is ascribed to the compressive residual stress applied to the embedded CNTs by the surrounding Al grains during the thermal cooling process [22,40,41]. CNTs and Al possess quite distinct coefficients of thermal expansion (CTEs). The CTE of Al is reported to be $23.6 \times 10^{-6}\,K^{-1}$ [23], while the reported CTEs of CNTs are generally considered to be close to zero [42] or even negative values [43]. The residual transverse stress applied on a reinforcing fiber in a matrix due to the mismatch of thermal expansion can be estimated using [40]

$$\sigma = \frac{CTE_m - CTE_f}{1/E_m + 1/E_f}\Delta T, \tag{4}$$

where CTE_m and CTE_f are the CTE of the metal matrix and the fiber, respectively; E_m and E_f are radial modulus of the matrix and the fiber, respectively; ΔT is the temperature change. The following parameters are employed in the calculation: $CTE_m = 23.6 \times 10^{-6}\,K^{-1}$ and $E_m = 69$ GPa for Al; $CTE_f = 1 \times 10^{-6}\,K^{-1}$ for CNT [40]; The effective radial modulus $E_f = 10$ GPa for DWCNTs (3.1 nm in outer diameter) [44]. For $\Delta T = 375$ K, the residual radial stress applied to the CNT is calculated to be 74 MPa for CNT-Al interfaces, which is substantially higher than the observed increase of the IFSS (about 6.6 MPa) due to thermally annealing. It is noted that the estimated thermal-induced residue stress is along the transverse direction of the CNT, which is perpendicular to the direction of the measured IFSS in the pull-out test. The data indicate a quite small frictional coefficient (less than 0.1) of the CNT-Al interface. We also want to point out that a residual stress might be developed during the metal film fabrication process, which may influence the interfacial load transfer. It is noted that the employed nanotubes have a much lower effective radial modulus than the matrix material and are more readily to deform transversely, even though they possess a higher longitudinal modulus. Therefore, substantial radial deformations are expected in the nanotube due to the residual compressive stress, which leads to a more intimate contact between the nanotube and the contacting Al grains. In addition, the asperity of local Al grains may enforce a substantial local deformation on the CNT surface, resulting in lock-in effects, and thus contributing to the interfacial load transfer and a higher interfacial strength. This envisioned lock-in effect is expected to be more prominent for nanotubes with a smaller number of walls that reportedly possess lower radial modulus [44,45].

Another possible mechanism that may lead to an increase of the CNT-Al interface after thermal-annealing is the formation of the reaction product on the interface. Thermogravimetric analysis (TGA) experiments show that a noticeable thermal oxidation of the employed DWCNTs starts at 450 °C in air. Therefore, the embedded CNTs inside the sandwiched thin-film nanocomposite were able to maintain their structural integrity when annealed at up to 400 °C. However, carbon atoms may react with Al atoms to form Al_4C_3 at elevated temperatures, which reportedly have a substantial influence on the interfacial strength. Prior studies report that the formation of this reaction product occurs at temperatures within a range from 500 °C to 660 °C (melting temperature of Al) [16,17,46]. Considering that the tested CNT-Al samples were annealed at a much lower temperature, it is highly possible that this reaction

product either did not exist or existed in a minimal quantity that has little or no influence on the interfacial strength. We performed XPS and Raman measurements to further investigate the presence/absence of Al_4C_3 in thermally annealed CNT-Al samples. Prior studies report the binding energies of 73.6 eV for Al(2p) and of 282.4 eV for C(1s) in Al_4C_3 [47]. However, none of these characteristic peaks were prominently exhibited in the Al(2p) and C(1s) x-ray photoelectron spectra that were acquired on the thermally annealed samples (see Figure S1 in Supporting Information). Raman analysis has also been used to identify the formation of Al_4C_3 after annealing process, showing two Al_4C_3 associated peaks at around 490 cm^{-1} and 855 cm^{-1} respectively [48]. None of those Al_4C_3 associated peaks were prominently exhibited in the recorded Raman spectra of CNT-Al samples before and after annealing (see Figure S2 in Supporting Information). Both XPS and Raman measurements consistently indicate the reaction product Al_4C_3 was either absent or existed in an extremely tiny, and probably undetectable, amount in thermally annealed CNT-Al samples, thus having little or no influence on the interfacial strength. The thermal annealing may also lead to a densification of the metal films and a thicker oxide layer on the surface of the Al grains in contact with CNTs due to the penetration of oxygen atoms through the Al film surface, the spacing between CNTs and Al grains, and/or even through CNTs that act as transport pipes. The resulting denser Al films and new or thicker Al_2O_3 layer on the CNT-Al interface lead to a more intimate contact between CNT surfaces and Al grains and/or the local lock-in effect, and thus contribute to its load transfer capacity and enhanced interfacial strength.

It is worth mentioning that the employed Al/CNT/Al sandwiched composite structure facilitates the experimental and theoretical investigation of the load transfer and the reinforcing mechanism in CNT-based MMNC; however, the CNT-Al interface in this model system is likely quite different from those in bulk MMNC manufactured for practical applications, which may go through various processing and densification steps, such as ball milling, hot pressing, rolling, forging and extrusion. All these complex processing steps may have substantial influences on the interfacial structure and strength. The work presented here represents an early-stage attempt in probing the CNT-Al binding phenomenon. More systematic studies of the binding interfaces in fiber-reinforced MMNC, including both experimental and modeling/simulation efforts, are warranted to further decipher the reinforcing mechanism by considering all of those complex manufacturing processes.

3. Conclusion

In summary, the mechanical strength of CNT-Al interfaces was characterized by using *in situ* electron microscopy nanomechanical single-tube pull-out techniques. The nanomechanical measurements reveal the shear lag effect on the CNT-Al interface and the effect of the thermal processing. The average IFSS of thermally annealed CNT-Al interfaces is found to be noticeably higher than the values for non-treated CNT-Al interfaces. The maximum load bearing capacity of the annealed interfaces is found to be substantially higher than that of the comparable non-annealed interfaces. The observed enhancement in mechanical strength of CNT-Al interfaces due to thermal annealing is ascribed in part to the compressive residual transverse stress applied to the embedded tube by the surrounding Al grains due to their substantial difference in thermal expansion coefficient. The findings are useful to better understand the load transfer mechanism in CNT-reinforced MMNC and how to better optimize the reinforcing performance through facile thermal processing.

4. Materials and methods

4.1. CNT-metal composite sample preparation and characterization

The employed double-walled carbon nanotubes (DWCNTs) were synthesized by chemical vapor deposition methods and purchased from Sigma-Aldrich. The nanotubes, originally in the form of dry powders, were firstly separated in deionized water using ultrasonication for 2 h with the aid of ionic surfactants [49]. The Al film was deposited at room temperature using an ATC Orion 8-E evaporator system (AJA International Inc.) with an Aluminum target of 99.999% in purity (Kamis Inc.) and a base vacuum of 1×10^{-8} torr. The CNT-Al sandwich structure was formed by first depositing a 100-nm-thick Al film on a fresh Si substrate, followed by spin-coating depositions of a well-dispersed nanotube solution and then the deposition of another Al film of 100 nm in thickness on top. The thermal annealing of the sandwiched composite sample was performed on top of a hot plate in ambient environment. The

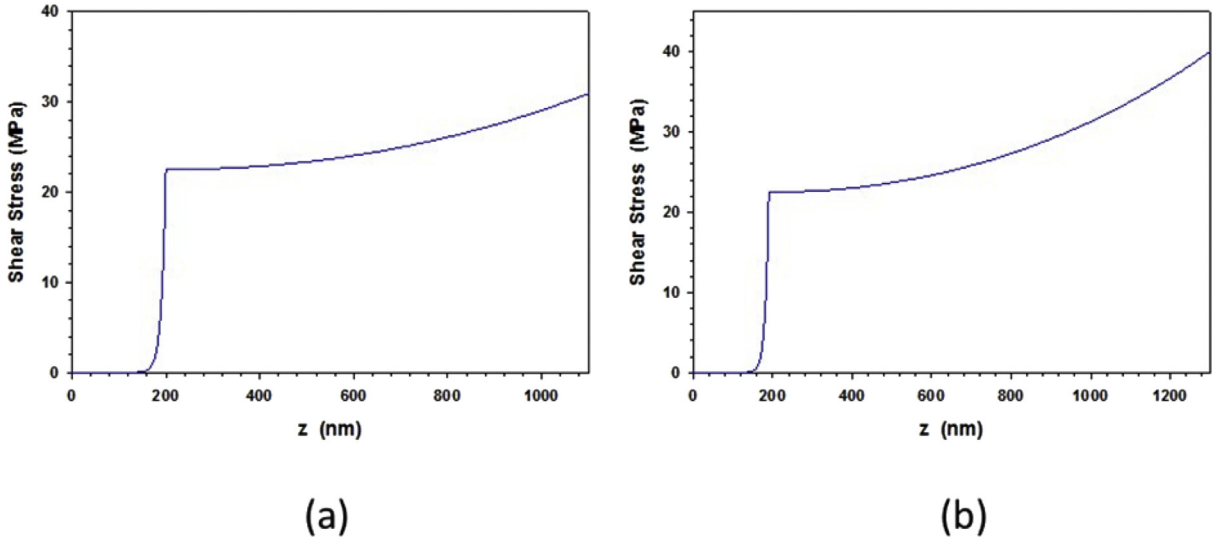

Fig. 7. Theoretically predicted interfacial shear stress distribution: (**a**) for a non-treated CNT-Al interface with an embedded tube length of 1100 nm; (**b**) for a thermally-treated interface with an embedded tube length of 1300 nm. (A colour version of this figure can be viewed online.)

sample was first heated to 400 °C at a rate of 2 °C/min and then held for 2 h. The cooling of the sample was controlled at a rate of 2 °C/min. A whole annealing cycle takes about 8 h and 15 min. The CNT-embedded thin-film composites (either with or without thermal annealing) were broken by means of cracking the substrate using a diamond scriber, and some of the embedded tubes were exposed as straight free-standing cantilever structures.

The AFM characterization of the dispersed CNTs and the deposited Al films were performed using a XE-70 AFM from Park Systems. The XPS characterization of the deposited Al and Al-CNT samples measurements were performed using a PHI 5000 VersaProbe instrument from Physical Electronics, Inc. Transmission electron microscopy (TEM) characterization of the CNT-Al composites with protruding tubes was performed using a JEM 2100F TEM (JEOL Ltd.).

4.2. *In situ* single-tube nanomechanical pull out measurements

The *in situ* nanomechanical single-tube pull-out tests were performed inside an FEI Nanolab 600 electron microscope by using an experimental scheme that has been previously demonstrated for the testing of the mechanical strength of CNT-polymer interfaces [31,33,34]. In brief, silicon AFM probes (model CSG 01, NT-MDT) were employed as the force sensors in the pull-out tests. The spring constant of each employed AFM probe was calibrated using thermal tuning methods [50] and was found to be within the range of 0.04–0.09 N/m. The AFM sensor was mounted to a 3D piezo stage that possesses 1 nm displace resolution in the X-Y-Z axes [35,51,52] and was controlled to move at a rate of approximately 0.5–1 μm/s. The embedded tube length was measured directly using the high resolution electron beam with a resolution of a few nanometers. The pull-out load was calculated based on the spring constant of the AFM force sensor and its last recorded deflection in the pull-out test with a resolution of about 0.5–1 nN.

Acknowledgements

This work was supported by US Air Force Office of Scientific Research - Low Density Materials program under Grant No FA9550-15-1-0491, and by National Science Foundation under Grant Nos. CMMI-1537333 and CMMI-1429176. We thank Dr. In-Tae Bae for his assistance with the TEM characterization. The SEM, TEM, XPS, and the single-tube pull-out measurements were performed using the facilities in the Analytical and Diagnostics Laboratory at Binghamton University's Small Scale Systems Integration and Packaging Center (S3IP). C.M.D acknowledges a fellowship support from the New York NASA Space Grant Consortium.

Appendix A. Supplementary data

Supplementary data related to this article can be found at http://dx.doi.org/10.1016/j.carbon.2017.09.020.

References

[1] S.R. Bakshi, D. Lahiri, A. Agarwal, Carbon nanotube reinforced metal matrix composites - a review, Int. Mater. Rev. (2013), http://dx.doi.org/10.1179/095066009X12572530170543.
[2] M. Haghshenas, Metal–matrix composites, in: Reference Module in Materials Science and Materials Engineering, Elsevier, 2016, http://dx.doi.org/10.1016/B978-0-12-803581-8.03950-3.
[3] F. Banhart, Interactions between metals and carbon nanotubes: at the interface between old and new materials, Nanoscale 1 (2009) 201–213, http://dx.doi.org/10.1039/B9NR00127A.
[4] M.L. Minus, H.G. Chae, S. Kumar, Single wall carbon nanotube templated oriented crystallization of poly(vinyl alcohol), Polymer 47 (2006) 3705–3710, http://dx.doi.org/10.1016/j.polymer.2006.03.076.
[5] Y. Zhang, K. Song, J. Meng, M.L. Minus, Tailoring polyacrylonitrile interfacial morphological structure by crystallization in the presence of single-wall carbon nanotubes, ACS Appl. Mater Interfaces 5 (2013) 807–814, http://dx.doi.org/10.1021/am302382m.
[6] X. Tao, L. Dong, X. Wang, W. Zhang, B.J. Nelson, X. Li, B4C-Nanowires/Carbon-Microfiber hybrid structures and composites from cotton t-shirts, Adv. Mater. 22 (2010) 2055–2059, http://dx.doi.org/10.1002/adma.200903071.
[7] S. Iijima, Helical microtubules of graphitic carbon, Nature 354 (1991) 56–58.
[8] M.S. Dresselhaus, Carbon Nanotubes, Springer, Berlin, 2001.
[9] T. Kuzumaki, K. Miyazawa, H. Ichinose, K. Ito, Processing of carbon nanotube reinforced aluminum composite, J. Mater. Res. 13 (1998) 2445–2449.
[10] C.L. Xu, B.Q. Wei, R.Z. Ma, J. Liang, X.K. Ma, D.H. Wu, Fabrication of aluminum–carbon nanotube composites and their electrical properties, Carbon 37 (1999) 855–858, http://dx.doi.org/10.1016/S0008-6223(98)00285-1.
[11] E. Flahaut, A. Peigney, C. Laurent, C. Marlière, F. Chastel, A. Rousset, Carbon nanotube–metal–oxide nanocomposites: microstructure, electrical conductivity and mechanical properties, Acta Mater. 48 (2000) 3803–3812, http://dx.doi.org/10.1016/S1359-6454(00)00147-6.
[12] D.A. Koss, R.R. Petrich, M.N. Kallas, J.R. Hellmann, Interfacial shear and matrix plasticity during fiber push-out in a metal-matrix composite, Compos. Sci. Technol. 51 (1994) 27–33, http://dx.doi.org/10.1016/0266-3538(94)90153-8.
[13] B.R. Kumar, T.S. Rao, AFM Studies on surface morphology, topography and texture of nanostructured zinc aluminum oxide thin films, Dig. J. Nanomater. Biostruct. 7 (2012) 1881–1889.
[14] L.-J. Meng, M.P. dos Santos, Direct current reactive magnetron sputtered zinc oxide thin films —the effect of the sputtering pressure, Thin Solid Films 250 (1994) 26–32, http://dx.doi.org/10.1016/0040-6090(94)90159-7.
[15] H. Kwon, G.-G. Lee, S.-G. Kim, B.-W. Lee, W.-C. Seo, M. Leparoux, Mechanical properties of nanodiamond and multi-walled carbon nanotubes dual-reinforced aluminum matrix composite materials, Mater. Sci. Eng. A 632 (2015) 72–77, http://dx.doi.org/10.1016/j.msea.2015.02.057.
[16] W. Zhou, S. Bang, H. Kurita, T. Miyazaki, Y. Fan, A. Kawasaki, Interface and interfacial reactions in multi-walled carbon nanotube-reinforced aluminum matrix composites, Carbon 96 (2016) 919–928, http://dx.doi.org/10.1016/j.carbon.2015.10.016.
[17] W. Zhou, T. Yamaguchi, K. Kikuchi, N. Nomura, A. Kawasaki, Effectively enhanced load transfer by interfacial reactions in multi-walled carbon nanotube reinforced Al matrix composites, Acta Mater. 125 (2017) 369–376, http://dx.doi.org/10.1016/j.actamat.2016.12.022.
[18] T. Kuzumaki, O. Ujiie, H. Ichinose, K. Ito, Mechanical characteristics and preparation of carbon nanotube fiber-reinforced Ti composite, Adv. Eng. Mater. 2 (2000) 416–418, http://dx.doi.org/10.1002/1527-2648(200007)2:7<416::AID-ADEM416>3.0.CO;2-Y.
[19] F. Mokdad, D.L. Chen, Z.Y. Liu, B.L. Xiao, D.R. Ni, Z.Y. Ma, Deformation and strengthening mechanisms of a carbon nanotube reinforced aluminum composite, Carbon 104 (2016) 64–77, http://dx.doi.org/10.1016/j.carbon.2016.03.038.
[20] L. Ci, Z. Ryu, N.Y. Jin-Phillipp, M. Rühle, Investigation of the interfacial reaction between multi-walled carbon nanotubes and aluminum, Acta Mater. 54 (2006) 5367–5375, http://dx.doi.org/10.1016/j.actamat.2006.06.031.
[21] S.R. Bakshi, A. Agarwal, An analysis of the factors affecting strengthening in carbon nanotube reinforced aluminum composites, Carbon 49 (2011) 533–544, http://dx.doi.org/10.1016/j.carbon.2010.09.054.
[22] R.J. Arsenault, N. Shi, Dislocation generation due to differences between the coefficients of thermal expansion, Mater. Sci. Eng. 81 (1986) 175–187, http://dx.doi.org/10.1016/0025-5416(86)90261-2.
[23] R. George, K.T. Kashyap, R. Rahul, S. Yamdagni, Strengthening in carbon nanotube/aluminium (CNT/Al) composites, Scr. Mater. 53 (2005) 1159–1163, http://dx.doi.org/10.1016/j.scriptamat.2005.07.022.
[24] Y. Xue, B. Jiang, L. Bourgeois, P. Dai, M. Mitome, C. Zhang, M. Yamaguchi, A. Matveev, C. Tang, Y. Bando, K. Tsuchiya, D. Golberg, Aluminum matrix composites reinforced with multi-walled boron nitride nanotubes fabricated by a high-pressure torsion technique, Mater. Des. 88 (2015) 451–460, http://dx.doi.org/10.1016/j.matdes.2015.08.162.
[25] E. Orowan, Zur kristallplastizität. III, Z. Phys. 89 (1934) 634–659, http://dx.doi.org/10.1007/BF01341480.
[26] F. Housaer, F. Beclin, M. Touzin, D. Tingaud, A. Legris, A. Addad, Interfacial characterization in carbon nanotube reinforced aluminum matrix composites, Mater. Charact. 110 (2015) 94–101, http://dx.doi.org/10.1016/j.matchar.2015.10.014.
[27] H. Kwon, M. Takamichi, A. Kawasaki, M. Leparoux, Investigation of the interfacial phases formed between carbon nanotubes and aluminum in a bulk material, Mater. Chem. Phys. 138 (2013) 787–793, http://dx.doi.org/10.1016/j.matchemphys.2012.12.062.
[28] C.F. Deng, D.Z. Wang, X.X. Zhang, A.B. Li, Processing and properties of carbon nanotubes reinforced aluminum composites, Mater. Sci. Eng. A 444 (2007) 138–145, http://dx.doi.org/10.1016/j.msea.2006.08.057.
[29] A.M.K. Esawi, M.A. El Borady, Carbon nanotube-reinforced aluminium strips, Compos. Sci. Technol. 68 (2008) 486–492, http://dx.doi.org/10.1016/j.compscitech.2007.06.030.
[30] W. Zhou, G. Yamamoto, Y. Fan, H. Kwon, T. Hashida, A. Kawasaki, In-situ characterization of interfacial shear strength in multi-walled carbon nanotube reinforced aluminum matrix composites, Carbon 106 (2016) 37–47, http://dx.doi.org/10.1016/j.carbon.2016.05.015.
[31] X. Chen, L. Zhang, M. Zheng, C. Park, X. Wang, C. Ke, Quantitative nanomechanical characterization of the van der Waals interfaces between carbon

nanotubes and epoxy, Carbon 82 (2015) 214–228, http://dx.doi.org/10.1016/j.carbon.2014.10.065.
[32] H.D. Espinosa, C.-H. Ke, Nanoelectromechanical systems - experiments and modeling, in: H.F.B. Bhushan (Ed.), Applied Scanning Probe Methods, Springer-Verlag, Heidelberg, 2006.
[33] X. Chen, M. Zheng, C. Park, C. Ke, Direct measurements of the mechanical strength of carbon nanotube–poly(methyl methacrylate) interfaces, Small 9 (2013) 3345–3351, http://dx.doi.org/10.1002/smll.201202771.
[34] X. Chen, L. Zhang, C. Park, C.C. Fay, X. Wang, C. Ke, Mechanical strength of boron nitride nanotube-polymer interfaces, Appl. Phys. Lett. 107 (2015), 253105, http://dx.doi.org/10.1063/1.4936755.
[35] C.H. Ke, N. Pugno, B. Peng, H.D. Espinosa, Experiments and modeling of carbon nanotube-based NEMS devices, J. Mech. Phys. Solids 53 (2005) 1314–1333.
[36] K. Lau, Interfacial bonding characteristics of nanotube/polymer composites, Chem. Phys. Lett. 370 (2003) 399–405, http://dx.doi.org/10.1016/S0009-2614(03)00100-3.
[37] B. Chen, S. Li, H. Imai, L. Jia, J. Umeda, M. Takahashi, K. Kondoh, Load transfer strengthening in carbon nanotubes reinforced metal matrix composites via in-situ tensile tests, Compos. Sci. Technol. 113 (2015) 1–8, http://dx.doi.org/10.1016/j.compscitech.2015.03.009.
[38] M. Borhani, F. Djavanroodi, Rubber pad-constrained groove pressing process: experimental and finite element investigation, Mater. Sci. Eng. A 546 (2012) 1–7, http://dx.doi.org/10.1016/j.msea.2012.02.089.
[39] S. Mahesh, J.C. Hanan, E. Üstündag, I.J. Beyerlein, Shear-lag model for a single fiber metal matrix composite with an elasto-plastic matrix and a slipping interface, Int. J. Solid Struct. 41 (2004) 4197–4218, http://dx.doi.org/10.1016/j.ijsolstr.2004.02.050.
[40] J.-P. Fan, D.-M. Zhuang, D.-Q. Zhao, G. Zhang, M.-S. Wu, F. Wei, Z.-J. Fan, Toughening and reinforcing alumina matrix composite with single-wall carbon nanotubes, Appl. Phys. Lett. (2006), http://dx.doi.org/10.1063/1.2336623.
[41] H.J. Choi, J.H. Shin, D.H. Bae, Grain size effect on the strengthening behavior of aluminum-based composites containing multi-walled carbon nanotubes, Compos. Sci. Technol. 71 (2011) 1699–1705, http://dx.doi.org/10.1016/j.compscitech.2011.07.013.
[42] C.F. Deng, Y.X. Ma, P. Zhang, X.X. Zhang, D.Z. Wang, Thermal expansion behaviors of aluminum composite reinforced with carbon nanotubes, Mater. Lett. 62 (2008) 2301–2303, http://dx.doi.org/10.1016/j.matlet.2007.11.086.
[43] Wenzhong Bao, Feng Miao, Zhen Chen, Hang Zhang, Wanyoung Jang, Chris Dames, Chun Ning Lau, Controlled ripple texturing of suspended graphene and ultrathin graphite membranes, Nat. Nanotechnol. 4 (2009) 562–566, http://dx.doi.org/10.1038/nnano.2009.191.
[44] M. Zheng, L. Zou, H. Wang, C. Park, C. Ke, Quantifying the transverse deformability of double-walled carbon and boron nitride nanotubes using an ultrathin nanomembrane covering scheme, J. Appl. Phys. (2012), http://dx.doi.org/10.1063/1.4766758.
[45] M. Zheng, C. Ke, I.-T. Bae, C. Park, M.W. Smith, K. Jordan, Radial elasticity of multi-walled boron nitride nanotubes, Nanotechnology 23 (2012), 095703, http://dx.doi.org/10.1088/0957-4484/23/9/095703.
[46] B. Chen, J. Shen, X. Ye, H. Imai, J. Umeda, M. Takahashi, K. Kondoh, Solid-state interfacial reaction and load transfer efficiency in carbon nanotubes (CNTs)-reinforced aluminum matrix composites, Carbon 114 (2017) 198–208, http://dx.doi.org/10.1016/j.carbon.2016.12.013.
[47] R. Hauert, J. Patscheider, M. Tobler, R. Zehringer, XPS investigation of the a-C:H/Al interface, Surf. Sci. 292 (1993) 121–129, http://dx.doi.org/10.1016/0039-6028(93)90395-Z.
[48] B. Chen, L. Jia, S. Li, H. Imai, M. Takahashi, K. Kondoh, In Situ synthesized Al4C3 nanorods with excellent strengthening effect in aluminum matrix composites, Adv. Eng. Mater 16 (2014) 972–975, http://dx.doi.org/10.1002/adem.201400232.
[49] M. Zheng, X. Chen, I.-T. Bae, C. Ke, C. Park, M.W. Smith, K. Jordan, Radial mechanical properties of single-walled boron nitride nanotubes, Small 8 (2012) 116–121, http://dx.doi.org/10.1002/smll.201100946.
[50] E.-L. Florin, M. Rief, H. Lehmann, M. Ludwig, C. Dornmair, V.T. Moy, H.E. Gaub, Sensing specific molecular interactions with the atomic force microscope, Biosens. Bioelectron. 10 (1995) 895–901, http://dx.doi.org/10.1016/0956-5663(95)99227-C.
[51] C.H. Ke, H.D. Espinosa, In situ electron microscopy electromechanical characterization of a bistable NEMS device, Small 2 (2006) 1484–1489.
[52] C. Ke, M. Zheng, G. Zhou, W. Cui, N. Pugno, R.N. Miles, Mechanical peeling of free-standing single-walled carbon nanotube bundles, Small 6 (2010) 438–445.